Inter-area oscillation statistical analysis of the U.S. Eastern interconnection

Yi Cui[1], Ling Wu[1], Wenpeng Yu[1], Yong Liu[1], Wenxuan Yao[1], Dao Zhou[1], Yilu Liu[1,2]

[1]*Department of Electrical Engineering and Computer Science, The University of Tennessee, Knoxville TN 37996, USA*
[2]*Oak Ridge National Laboratory, Oak Ridge, TN 37831, USA*
E-mail: ycui17@utk.edu

Published in *The Journal of Engineering*; Received on 9th June 2017; Revised on 25th August 2017; Accepted on 29th September 2017

Abstract: Although extensive studies have been conducted on inter-area oscillation detection and analysis by using phasor measurement data, few have focused on inter-area oscillation statistics due to the lack of considerably long-term and high-resolution recorded data. A preliminary statistical analysis on the inter-area oscillations that occurred in the U.S. Eastern interconnection from 2010 to 2015 is presented. These oscillation events were captured and recorded by the wide-area frequency monitoring network FNET/GridEye. Oscillation occurrence, dominant frequency, damping ratio and oscillation excitation types are investigated to explore the statistical characteristics of the detected inter-area oscillations. The results from this paper will provide valuable information for system operators and planners regarding network operation and future grid development.

1 Introduction

Inter-area oscillation is a critical issue that limits the power transfer capability of transmission lines and threatens the stability of power systems. Therefore, it is of significance to understand and damp inter-area oscillations for the stable operation of power grids. Over the past several decades, wide-area monitoring system (WAMS) has been developed to detect disturbances of large interconnected grids and monitor the power system dynamics by using global positioning system (GPS)-synchronised phasor measurement units (PMUs) [1]. Extensive studies have been conducted based on the measured phasor data regarding: (i) inter-area oscillation detection, (ii) oscillation mode identification [2, 3], and (iii) oscillation damping control [3, 4] to achieve proper damping controls and improving power system small-signal stability.

Inter-area oscillation detection is usually achieved by screening the real-time stream of PU data and detecting the presence of oscillation within a small data window by using a variety of techniques, pre-selected threshold values, and decision rules [5]. Typical oscillation detection algorithms in the literature include wavelet transform (WT)-based methods [6], Hilbert transform methods [7], spectral Kurtosis analysis [8], Kalman filter-based approaches [9], and other artificial intelligence methods [10]. However, to achieve online detection of inter-area oscillations within the shortest time frame, some straightforward oscillation identification applications with low calculation burdens have been employed in the field [11].

The oscillation signal usually contains several modes with different frequency and damping ratios. It is vital to extract dominant modes from the detected oscillations for online damping controls and small-signal stability improvement [12–14]. Traditionally, oscillation modes are obtained by a linearised model, which is derived from the detailed system model at a specific operating point. However, such system model may not be accurate due to the changes in the network topology and operating conditions. To overcome the above limitations, measurement-based mode identification approaches are proposed and widely used by utilities for oscillation mode estimation. Typical mode identification approaches based on the PUs include Prony method [15], matrix pencil (MP) method [16], empirical mode decomposition [17], autoregressive moving average block-processing method [18], and state-space subspace system identification (N4SID) algorithm [19, 20]. The fundamental of the above mode identification methods is based on transfer function, which directly estimates the mode of oscillations by treating the measurements (e.g. frequency and voltage angle) as the outputs of the system [17].

Recent works regarding to the oscillation identification involves cross-correlation-based method, which can remove the difficulties of order determination and parameters initialisation in the original Prony method [21]. In [22], data and information fusion techniques are integrated with Prony method to improve the computational efficiency for mode identification, and in [23] multiple Prony models are investigated to explore the true modes that are consistently present in the ring-down oscillations. A stepwise regression method is applied to automatically identify the dominant modes from Prony analysis [24]. To improve estimation accuracy on damping ratio, a parametric discrete Fourier transform-based (FT) method is proposed by analysing two sets of ring-down frequency data with oscillation against each other [25]. A Bayesian approach is also developed to identify the modal parameters based on their uncertainties using ambient PMU measurements [26]. Other improved methods for oscillation identification are also developed including adaptive local iterative filtering decomposition [27], digital Taylor–FT [28], extended Kalman filter [29], and adaptive stochastic subspace identification [30].

Although extensive studies have been conducted on inter-area oscillations detection and analysis by using PU data, there are almost no studies to explore the statistical characteristics of oscillations due to the lack of recorded high-resolution PUs over multiple years. As a pilot WAMS system, frequency monitoring network FNET/GridEye has been monitoring the U.S. power grids for more than a decade and many terabytes' (TB') PU data have been archived. To take advantage of those valuable data, a preliminary statistical analysis on the historical inter-area oscillations in the U.S. Eastern interconnection (EI) is provided in this paper to discover the features of the EI system inter-area oscillations. More than 20,000 inter-area oscillations captured by FNET/GridEye are analysed and oscillation occurrence, dominant frequency, damping ratio and how the oscillations were excited are investigated to explore the statistical characteristics of the detected inter-area oscillations. It is expected that the information in this paper will provide valuable statistics to system operators and planners for evaluating power system stability, determining damping controls strategies and developing future network plans.

This paper is organised as follows: Section 2 introduces the inter-area oscillation detection and mode identification techniques employed by FNET/GridEye; Sections 3–5 present the statistical analysis of inter-area oscillation occurrences, dominant mode

frequency, damping ratio and oscillation excitation types, respectively; and Section 6 concludes this paper.

2 Methodology of inter-area oscillation detection and mode identification by FNET/GridEye

2.1 Overview of FNET/GridEye

FNET/GridEye is a pilot wide-area frequency monitoring system with high accuracy (±0.005° phase angle accuracy), which is implemented at the distribution level of power grids [11, 31]. To collect GPS-synchronised PU, a large number of easily installed low-cost frequency disturbance recorders (FDRs) are connected to the single-phase 120 V electrical outlets at different locations.

Fig. 1 shows the architecture of FNET/GridEye system [11] and the latest deployment of FDR in North America is shown in Fig. 2. For now, there are 233 FDR units installed in EI by which frequency, voltage magnitude, and voltage phase angle are continuously measured to provide real-time awareness of power system situations. Accompanied by FDR units' deployment, a series of advanced situation awareness tools have been successfully developed and implemented to process high volume of real-time PU data. Since 2003, the FNET/GridEye monitors system situations of more than tens of electric utilities in North America and a big amount of PUs regarding system's behaviours and operations were archived by the FNET/GridEye servers hosted at the University of Tennessee at Knoxville (UTK) and Oak Ridge National Laboratory. This paper mainly focuses on the statistical analysis of 20,040 inter-area oscillations of EI network, which were detected from five TBs' PU data archived in FNET/Grid system from 2010 to 2015.

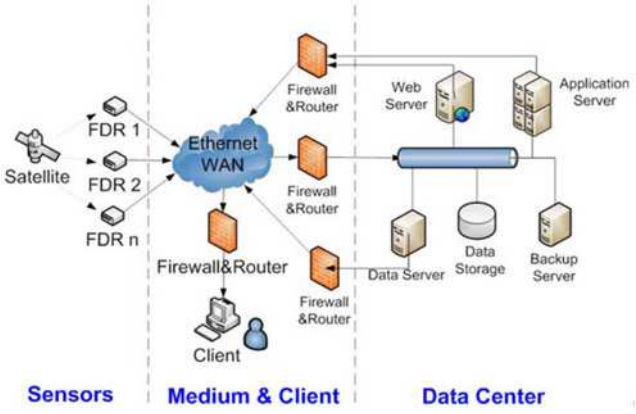

Fig. 1 *Structure of FNET/GridEye system hosted by the UTK, TN, USA*

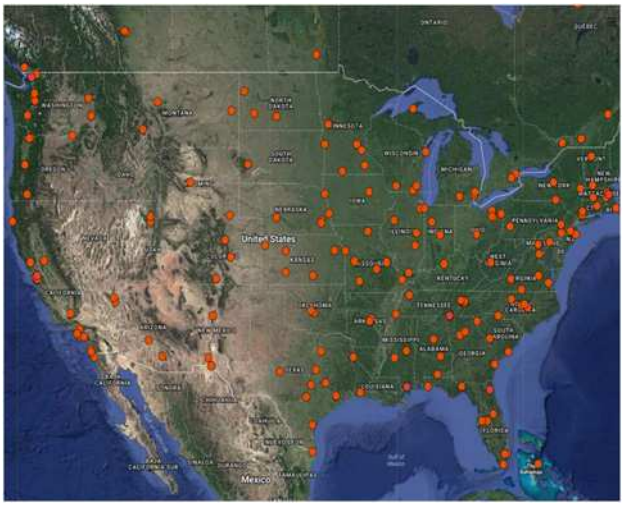

Fig. 2 *Deployment of FDR in North America*

2.2 Methodology of inter-area oscillation detection

FNET/GridEye uses the derivative of phase angles measured by each FDR unit to detect inter-area oscillations. It has the capability to achieve an online detection of inter-area oscillations. In data pre-processing step, the absolute phase angle measured by a number of FDRs installed at different areas of the system is unwrapped and the relative phase angles of each FDR unit are calculated by subtracting the angle measured by the pre-defined reference FDR unit from phase angles measured by other FDRs. Then, such relative angles are fed into oscillation detection module to determine whether an oscillation occurs in the system.

Fig. 3 illustrates the two-step approach of online oscillation detection by FNET/GridEye. To detect a disturbance, the first step is to calculate relative angle rise or drop within the latest 3 s (shown as time window 1 in Fig. 3). Once the magnitude of angle rise or drop exceeds pre-defined threshold 1, the oscillation detection module will try to calculate the angle difference between the maximum angle value within the next 5 s and the minimum angle value between the time of the maximum angle and the end of the 5 s (shown as time window 2 in Fig. 3). If the difference in magnitude of the maximum and minimum angle is beyond threshold 2, this time window is considered as containing a potential oscillation event. The threshold values (thresholds 1 and 2) for oscillation detection are justified empirically by analysing historically archived event cases in FNET system. To avoid false alarms caused by measurement noises, a voting strategy is employed by FNET/GridEye that at least two FDR units detect the disturbance in the same time window; the oscillation can be finally confirmed.

Once an oscillation is detected, the system automatically sends alerts to operators with a comprehensive report (as shown in Fig. 4) containing oscillation occurrence time, frequency, and relative angle of involved FDR units, largest oscillation amplitude, oscillation frequency, damping ratio etc.

2.3 Methodology of inter-area oscillation mode identification

FNET/GridEye online oscillation detection application detects low-frequency oscillations, and analyses the oscillation mode using multi-channel MP (MMP) method [16]. There are some advantages of MMP over Prony analysis and wavelet-based methods for mode identification: (i) MMP can extract the signal poles directly from the eigenvalues of a single-developed matrix, whereas for other methods such as Prony analysis usually requires two steps (i.e. discrete linear prediction model construction and roots calculation of the characteristic polynomial) to identify the oscillation mode.

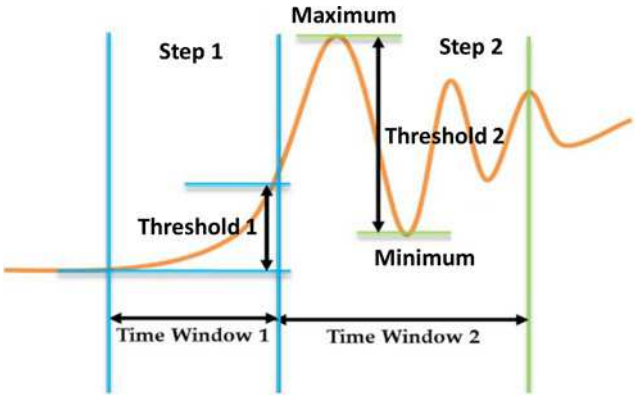

Fig. 3 *Illustration of two-step approach for oscillation event detection*

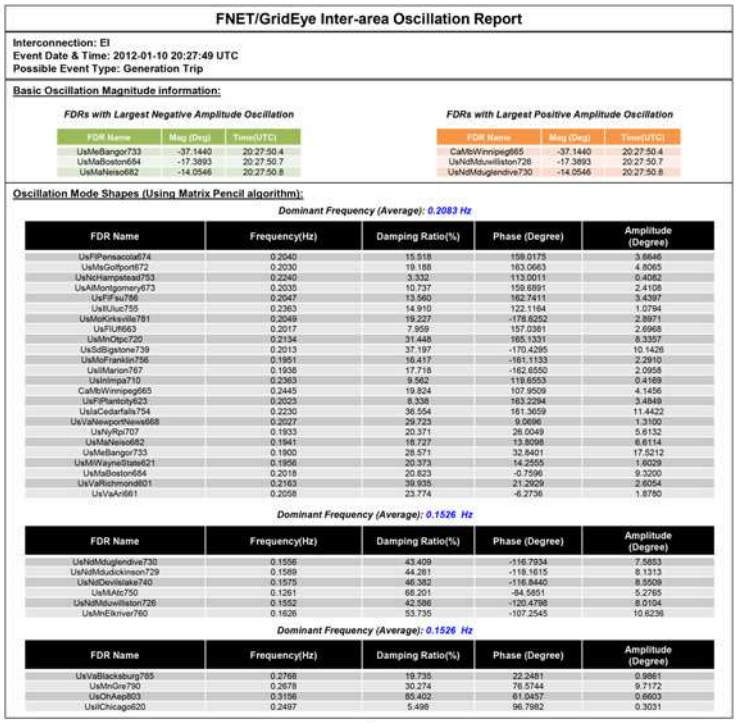

FNET/GridEye Inter-area Oscillation Report

Interconnection: EI
Event Date & Time: 2012-01-10 20:27:49 UTC
Possible Event Type: Generation Trip

Basic Oscillation Magnitude information:

FDRs with Largest Negative Amplitude Oscillation

FDR Name	Mag (Deg)	Time(UTC)
UsMeBangor733	-37.1440	20:27:50.4
UsMaBoston684	-17.3893	20:27:50.7
UsMaNelso682	-14.0546	20:27:50.8

FDRs with Largest Positive Amplitude Oscillation

FDR Name	Mag (Deg)	Time(UTC)
CaMbWinnipeg665	-37.1440	20:27:50.4
UsNdMduwilliston726	-17.3893	20:27:50.7
UsNdMduglendive730	-14.0546	20:27:50.8

Oscillation Mode Shapes (Using Matrix Pencil algorithm):

Dominant Frequency (Average): 0.2083 Hz

FDR Name	Frequency(Hz)	Damping Ratio(%)	Phase (Degree)	Amplitude (Degree)
UsFlPensacola674	0.2040	15.518	159.0175	3.6646
UsMsGolfport672	0.2030	19.188	163.0663	4.8065
UsNcHampatesa753	0.2240	3.332	113.0011	0.4082
UsAlMontgomery673	0.2035	10.737	159.6891	2.4108
UsFlFau786	0.2047	13.560	162.7411	3.4397
UsILUiuc755	0.2363	14.910	122.1184	1.0794
UsMoKirksville781	0.2049	19.227	-178.6252	2.8971
UsFlUf663	0.2017	7.959	157.0381	2.6968
UsMnOtpc720	0.2134	31.448	165.1331	8.3357
UsSdBigstone739	0.2013	37.197	-170.4295	10.1426
UsMoFranklin736	0.1951	16.417	-161.1133	2.2910
UsILMarion767	0.1938	17.718	-162.6550	2.0958
UsInImpa710	0.2363	9.562	119.6553	0.4189
CaMbWinnipeg665	0.2445	19.824	107.9509	4.1456
UsFlPlantcity623	0.2023	8.336	163.2294	3.4849
UsIaCedarfalls754	0.2230	36.554	161.3659	11.4422
UsVaNewportNews668	0.2027	29.723	9.0696	1.3100
UsNyRpi707	0.1933	20.371	28.0049	5.6132
UsMaNelso682	0.1941	18.727	13.8098	6.6114
UsMeBangor733	0.1900	28.571	32.8401	17.5212
UsMiWayneState621	0.1956	20.373	14.2555	1.8029
UsMaBoston684	0.2018	20.823	-0.7596	9.3200
UsVaRichmond801	0.2163	39.935	21.2929	2.6054
UsVaAvri661	0.2058	23.774	-6.2736	1.8780

Dominant Frequency (Average): 0.1526 Hz

FDR Name	Frequency(Hz)	Damping Ratio(%)	Phase (Degree)	Amplitude (Degree)
UsNdMduglendive730	0.1556	43.409	-116.7934	7.5853
UsNdMdudickinson729	0.1589	44.261	-118.1615	8.1313
UsNdDevilslake740	0.1575	46.382	-116.8440	8.5509
UsMiMtc750	0.1261	68.201	-84.5851	5.2765
UsNdMduwilliston726	0.1552	42.586	-120.4798	8.0104
UsMnElkriver760	0.1626	53.735	-107.2545	10.6236

Dominant Frequency (Average): 0.1526 Hz

FDR Name	Frequency(Hz)	Damping Ratio(%)	Phase (Degree)	Amplitude (Degree)
UsVaBlacksburg765	0.2768	19.735	22.2481	0.9861
UsMnGre790	0.2678	30.274	76.5744	9.7172
UsOhAsp803	0.3156	85.402	61.0457	0.8603
UsIlChicago820	0.2497	5.498	96.7982	0.3031

a

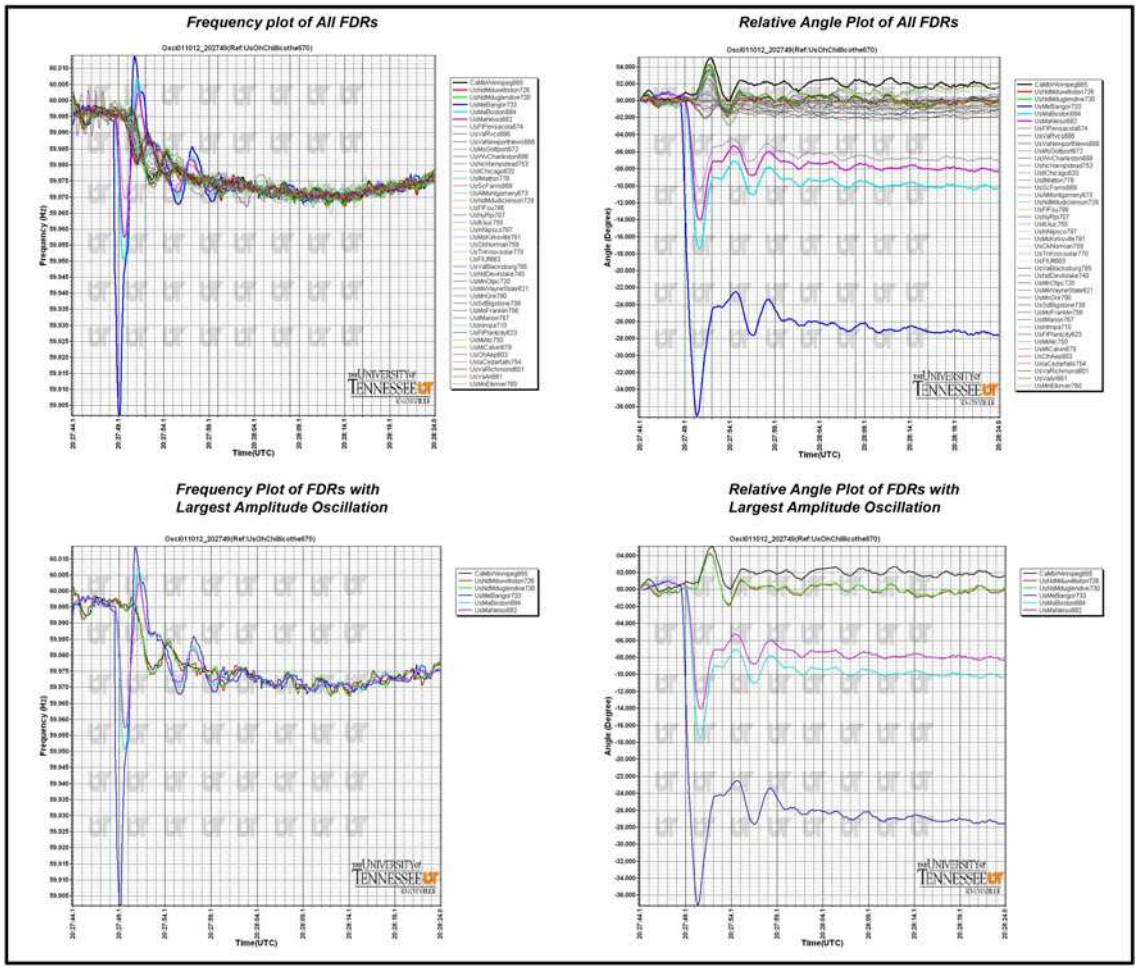

b

Fig. 4 *Oscillation analysis report from FNET/GridEye*
a Mode identification results in oscillation analysis report from FNET/GridEye
b Event data plots in oscillation analysis report

doi: 10.1049/joe.2017.0243

Wavelet-based method may also require a proper selection on the mother wavelet signals for mode analysis; (ii) MMP uses the generalised eigenvalue solution to find signal poles, which remove the limitation on the number of poles. However, the Prony method may have some difficulties in calculating the roots of a polynomial when the pole number is >50 [32]; and (iii) MMP has a high robustness in oscillation mode identification, especially when noise or interferences are involved in frequency measurements and it also shows a high computation efficiency and thus can be implemented as an online application to provide oscillation modes information in real time.

The MP method fits a sum of damped sinusoids to the oscillation signal as shown in (1)

$$y(t) = \sum_{k=1}^{N} \boldsymbol{R}_k \mathrm{e}^{\lambda_k t} = \sum_{k=1}^{N} R_k \mathrm{e}^{(-\alpha_k + \mathrm{j}\beta_k)t} = \sum_{k=1}^{N} R_k \mathrm{e}^{-\alpha_k} \sin(\beta_k t + \theta_k) \tag{1}$$

where the $y(t)$ denotes the detected oscillation signal and it equals to the sum of the product of the residues or complex amplitudes $\boldsymbol{R}_k$ and the poles $\mathbf{e}^{\lambda_k t}$, $\boldsymbol{\lambda}_k$ denote the eigenvector of the state matrix.

If the oscillation signal is sampled with fixed time step, (1) can be rewritten as (2)

$$[\boldsymbol{Y}] = \begin{bmatrix} y(0) \\ y(1) \\ \cdots \\ y(N-1) \end{bmatrix} = \begin{bmatrix} 1 & 1 & \cdots & 1 \\ z_1 & z_2 & \cdots & z_N \\ \cdots & \cdots & \ddots & \cdots \\ z_1^{N-1} & z_2^{N-1} & \cdots & z_N^{N-1} \end{bmatrix} \begin{bmatrix} \boldsymbol{R}_1 \\ \boldsymbol{R}_2 \\ \cdots \\ \boldsymbol{R}_N \end{bmatrix} \tag{2}$$

where $z_k = \mathrm{e}^{\lambda_k \times \Delta t}$.

The MP method is dedicated to construct a matrix pair $\boldsymbol{Y}_1^{-1}\boldsymbol{Y}_2$ as (3) and (4), whose eigenvalues are z_k

$$\boldsymbol{Y}_1 = \begin{bmatrix} y(0) & y(1) & \cdots & y(L-1) \\ y(1) & y(2) & \cdots & y(L) \\ \cdots & \cdots & \ddots & \cdots \\ y(N-L-1) & y(N-L) & \cdots & y(N-2) \end{bmatrix} \tag{3}$$

$$\boldsymbol{Y}_2 = \begin{bmatrix} y(1) & y(2) & \cdots & y(L) \\ y(2) & y(3) & \cdots & y(L+1) \\ \cdots & \cdots & \ddots & \cdots \\ y(N-L) & y(N-L+1) & \cdots & y(N-1) \end{bmatrix} \tag{4}$$

MMP uses singular value decomposition on $[\boldsymbol{Y}]$ to obtain the eigenvectors as (5)

$$[\boldsymbol{Y}] = [\boldsymbol{U}][\boldsymbol{S}][\boldsymbol{V}^{\mathrm{T}}] \tag{5}$$

where $[\boldsymbol{U}]$ and $[\boldsymbol{V}]$ denote unitary matrices consisting of eigenvectors of $[\boldsymbol{Y}^{\mathrm{T}}][\boldsymbol{Y}]$ and $[\boldsymbol{Y}][\boldsymbol{Y}^{\mathrm{T}}]$, $[\boldsymbol{S}]$ denote the diagonal matrix containing singular values of $[\boldsymbol{Y}]$. By substituting (3) and (4) into (5), (6) and (7) can be obtained

$$[\boldsymbol{Y}_1] = [\boldsymbol{U}][\boldsymbol{S}][\boldsymbol{V}_1]^{\mathrm{T}} \tag{6}$$

$$[\boldsymbol{Y}_2] = [\boldsymbol{U}][\boldsymbol{S}][\boldsymbol{V}_2]^{\mathrm{T}} \tag{7}$$

where $[\boldsymbol{V}_1] = [v_1, v_2, \ldots, v_{N-1}]$ and $[\boldsymbol{V}_2] = [v_2, v_3, \ldots, v_N]$.

The poles of the signal can be calculated by non-zero eigenvalues of (8)

$$[\boldsymbol{Y}_2] - \lambda[\boldsymbol{Y}_1] = [\boldsymbol{Z}_1][\boldsymbol{R}]\{[\boldsymbol{Z}_0] - \lambda[\boldsymbol{I}]\}[\boldsymbol{Z}_2] \tag{8}$$

where

$$[\boldsymbol{Z}_0] = \mathrm{diag}[z_1, z_2, \ldots, z_M] \tag{9}$$

$$[\boldsymbol{Z}_1] = \begin{bmatrix} 1 & 1 & \cdots & 1 \\ z_1 & z_2 & \cdots & z_M \\ \cdots & \cdots & \ddots & \cdots \\ z_1^{N-L-1} & z_2^{N-L-1} & \cdots & z_M^{N-L-1} \end{bmatrix} \tag{10}$$

$$[\boldsymbol{Z}_2] = \begin{bmatrix} 1 & z_1 & \cdots & z_1^{L-1} \\ 1 & z_2 & \cdots & z_2^{L-1} \\ \cdots & \cdots & \ddots & \cdots \\ 1 & z_M & \cdots & z_M^{L-1} \end{bmatrix} \tag{11}$$

Once the roots of z_k in (2) are obtained, the amplitude, phase angle, frequency, and damping ratio of each damped sinusoid in (1) can be further determined. The MMP analysis results are incorporated in the FNET/GridEye oscillation report as shown in Fig. 4.

3 Inter-area oscillation occurrence analysis

This paper focuses on the statistical analysis of captured inter-area oscillations with significant magnitudes in EI. The EI system is the largest interconnection in North America, which consists of more than 3000 generators operated by 36 balancing authorities including Pennsylvania–Jersey–Maryland (PJM), Midcontinent Independent System Operator (ISO), New York ISO etc. [33]. This section presents a statistical analysis on the monthly and hourly occurrences of inter-area oscillations in EI.

3.1 Monthly occurrence

The monthly distribution of the EI oscillation occurrence from 2010 to 2015 is shown in Fig. 5. The average oscillation occurrence number for each month is also presented as blue circles. It can be seen that there is a similar trend in monthly oscillation occurrence distribution over 6 years, except the year 2013 when there was a significant increase from January to February. It has to be investigated further in order to find out the possible causes for this inconsistency.

By comparing the average oscillation occurrence number for different months, it shows that most oscillations were detected in October while fewest were detected in January. This discovery seems to contradict with the conception that oscillations are more

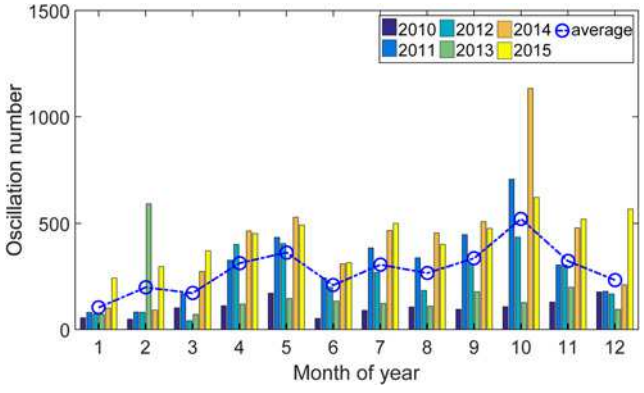

Fig. 5 *Monthly occurrence of inter-area oscillations in EI*

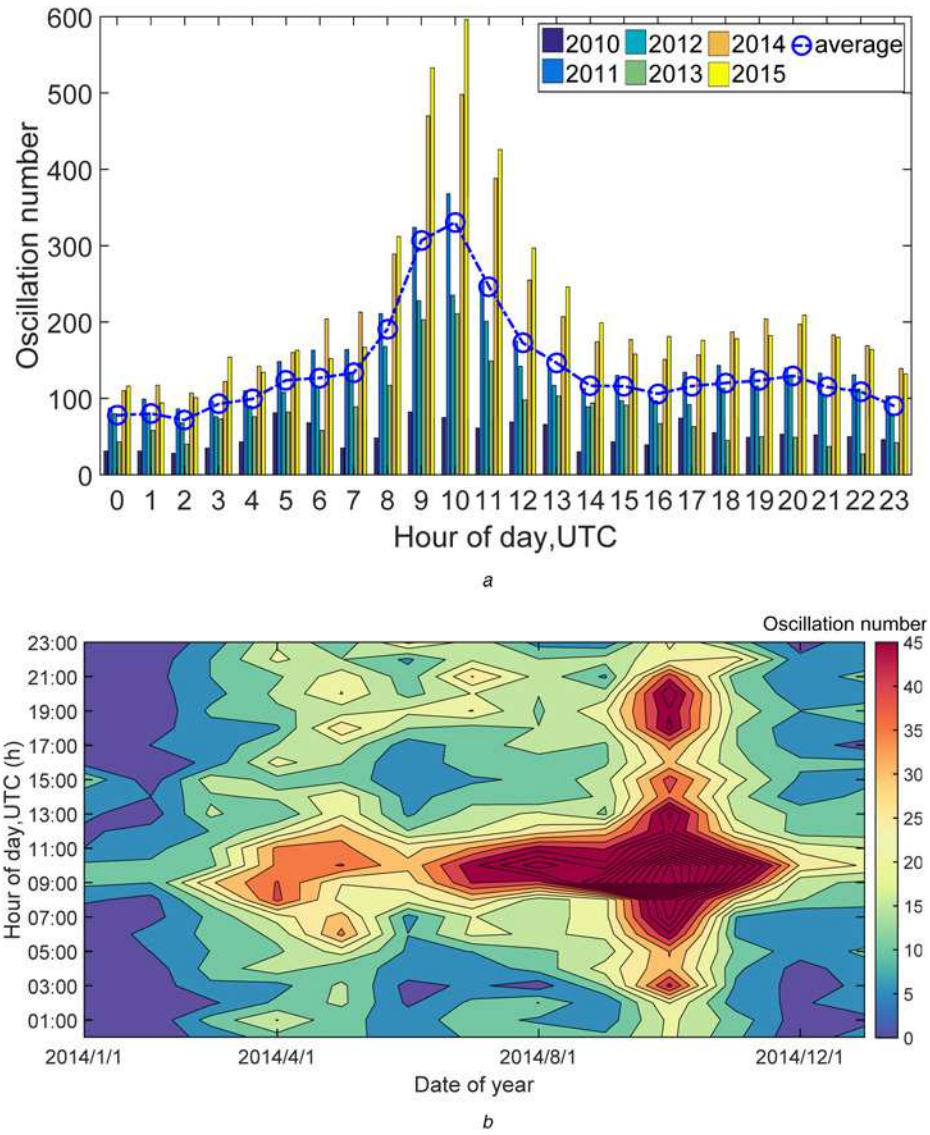

Fig. 6 *Hourly occurrence of inter-area oscillations in EI*
a Hourly overall occurrence of inter-area oscillations from 2010 to 2015
b Hourly occurrence of inter-area oscillations in 2014

common in peak seasons when the system is more stressed. One possible explanation is that both system generation and load during shoulder seasons are smaller than those of peak seasons, which make the system a relatively smaller one during shoulder seasons. Owing to smaller system size and inertia, a disturbance may trigger more severe oscillations. That may explain why more oscillations were detected during shoulder reasons than peak seasons. Further studies must be carried out to further look into this phenomenon.

3.2 Hourly occurrence

Hourly distribution of the EI inter-area oscillations is shown in Fig. 6. It can be observed that all 6 years from 2010 to 2015 share similar trends regarding the hourly oscillation occurrence distribution. Generally, the number of detected oscillations started to increase from 8 am coordinated universal time (UTC) time and reached its peak around 10 am UTC time. To clearly present the intra-year changes in the oscillation number, Fig. 6*b* shows a contour map of oscillation occurrence which is grouped by 24 h of a day through the whole year of 2014. From Fig. 6*b*, it can be seen that the oscillation occurrence has a clear seasonal difference and hourly variation. For a single hour, the maximum oscillation number is 45, which occurred at 10 am UTC time in October,

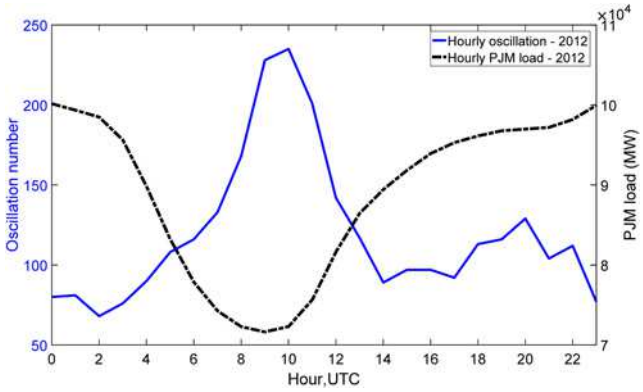

Fig. 7 *Correlation between hourly distribution of EI oscillation and PJM load in 2012*

Table 1 Correlation coefficient between hourly occurrence of inter-area oscillations in EI and PJM load

Year	2012	2013	2014	2015
correlation coefficient	−0.80	−0.81	−0.79	−0.73

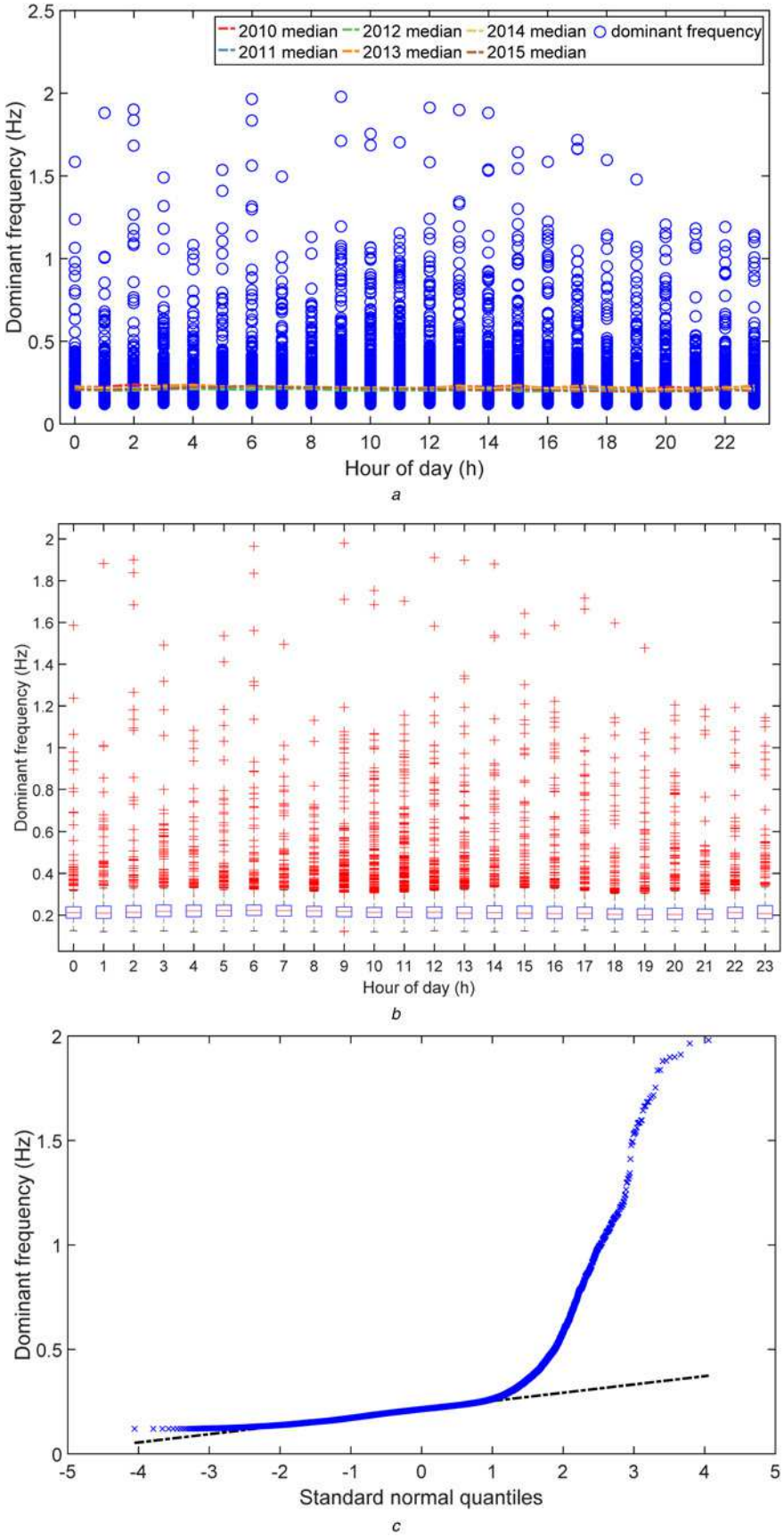

Fig. 8 *Dominant frequency distribution of inter-area oscillations in EI*
a Scatter plot of dominant frequency and median value in each hour of a day
b Boxplot of dominant frequency distribution
c *Q*–*Q* plot of dominant frequency distribution

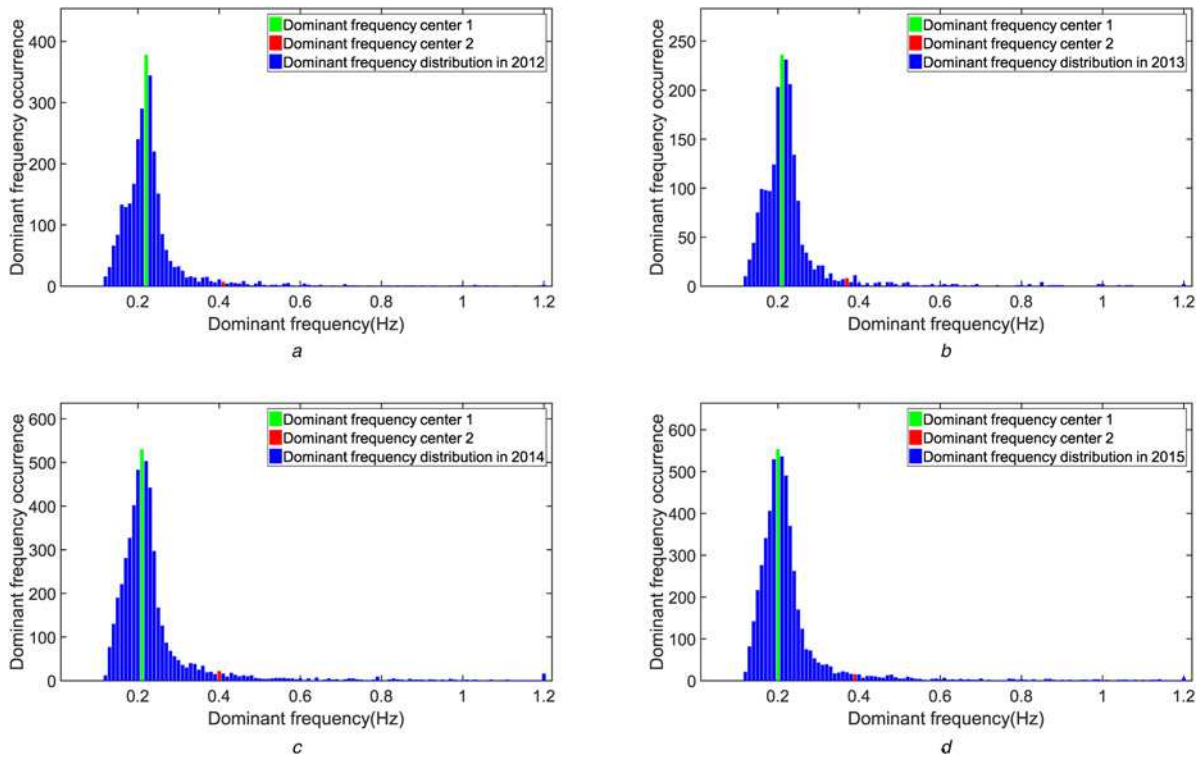

Fig. 9 *Dominant frequency distribution of annual inter-area oscillations in EI*
a Dominant frequency distribution of EI in 2012
b Dominant frequency distribution of EI in 2013
c Dominant frequency distribution of EI in 2014
d Dominant frequency distribution of EI in 2015

whereas during January, minimal oscillations have been detected for each hour.

To find out any possible correlation between oscillation number and daily loading profile, hourly oscillation distribution and PJM load profile are plotted together in Fig. 7. PJM accounts for roughly one quarter of the EI system's total load and thus can be representative of the total EI load. Considering the EI load profile also has seasonal characteristics, the median value of hourly loads throughout a whole year was calculated.

Fig. 7 shows the correlation between hourly occurrence of inter-area oscillations in EI and PJM load in 2012. It can be seen that more oscillations were detected when the system load were smaller (less system generation and lower system inertia). A correlation coefficient between hourly occurrence of inter-area oscillations in EI and PJM daily load is also calculated for each year, as given in Table 1. All these results strongly indicate that oscillation occurrence is highly correlated with system load and size. This phenomenon may be also explained by the fact that a disturbance can potentially cause more severe oscillations in a smaller system.

Fig. 7 shows the correlation between hourly occurrence of inter-area oscillations in EI and PJM load from 2012 to 2015. From Fig. 7, it can be seen that more oscillations are detected from 8 am to 10 am UTC time when the system load is lower. The small difference between the hours of PJM load valley and the hours of oscillation occurrence peak is possibly caused by the mismatch of load profile between EI system and PJM grids. However, it still strongly indicates the oscillation occurrence is highly correlated with the system load. The magnitude of correlation coefficient between hourly occurrence of inter-area oscillations in EI and PJM daily load is ~0.8 as shown in Table 1. This phenomenon can be also explained as that a disturbance can potentially cause more severe frequency deviations under light-loaded conditions. Therefore, more oscillations are detected during the light-load hours using the same oscillation detection tool from FNET/GridEye.

4 Inter-area oscillation mode analysis

Oscillation mode frequency and damping ratio are the two crucial parameters of inter-area oscillations. According to (1), an oscillation signal can be decomposed into different components (modes) over the frequency spectrum, where each mode is denoted as a sinusoid signal with a specific frequency. Among various oscillation modes, only the dominate mode that contains the most energy determines the oscillation signal predominately [34]. Particularly, if the dominate mode frequency is close to system natural frequency, generators, and other equipments may be influenced and even damaged. Therefore, this section focuses on the statistical analysis on the dominant mode frequency of the inter-area oscillation from 2010 to 2015.

Fig. 8*a* shows the hourly distribution of dominant mode frequency distribution in EI from 2010 to 2015. Median values of dominant mode frequency for each hour are presented by dash lines with different colours. From Fig. 8, it can be observed that most oscillations' dominant mode frequency in EI is smaller than 0.4 Hz. Minimal difference can be observed in different hours. The median frequencies of each hour are similarly around 0.2 Hz, and the yearly difference in median frequency is minimal. Similar

Table 2 Dominant frequency centroids of oscillations in EI

Year	Dominant frequency centre 1, Hz	Dominant frequency centre 2, Hz
2010	0.21	0.38
2011	0.22	0.41
2012	0.22	0.41
2013	0.21	0.37
2014	0.21	0.41
2015	0.20	0.41

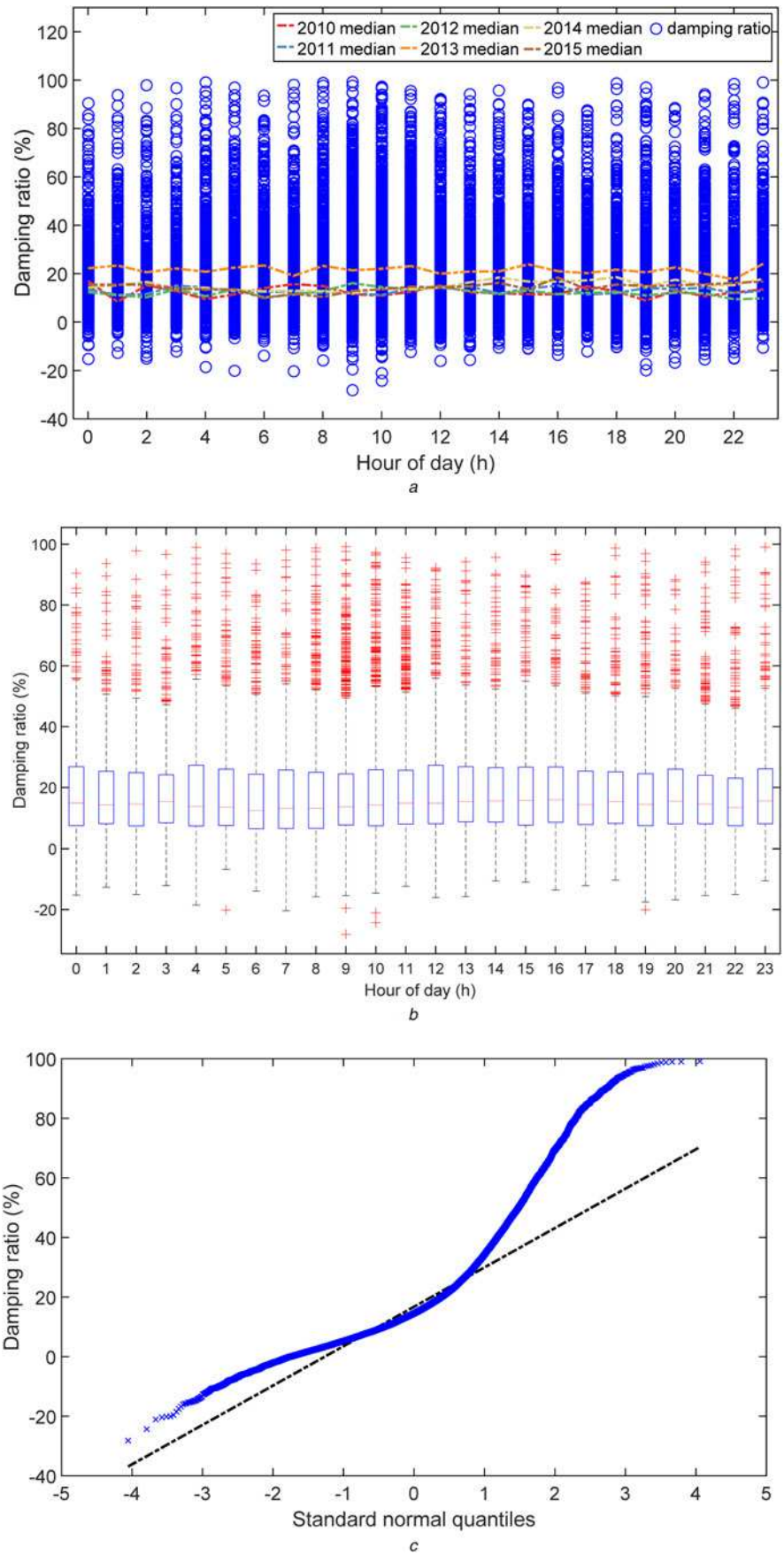

Fig. 10 *Damping ratio distribution of inter-area oscillations in EI*
a Scatter plot of damping ratio and median value in each hour of a day
b Boxplot of damping ratio distribution
c *Q*–*Q* plot of damping ratio distribution

statistical analysis was performed by grouping dominant mode frequency into 12 months. The monthly distribution of dominant mode frequency produces similar conclusions to the hourly distribution. In a word, no obvious daily and seasonal characteristics of oscillation dominant mode frequency have been discovered for the EI system.

To further explore the distribution of the dominant frequency, Fig. 8*b* shows the boxplot of dominant frequency distribution in each hour through 6 years. Fig. 8*c* presents a quantile–quantile plot (*Q*–*Q* plot) of the dominant frequency during the 6 years period. From Fig. 8*c*, it can be seen that the region of dominant frequency close to 0.2 Hz clearly shows a normal distribution, as in this part the quantile curve of dominant frequency (marked as blue '×' in Fig. 8*c*) closely coincides with the normal distribution curve (black dash-dot line). In addition, the tendency of the medium to high dominant frequency (above 0.4 Hz) has significantly deviated from the normal distribution. This is illustrated as a heavy-tailed distribution in the *Q*–*Q* plot, which suggests the probability for a dominant frequency deviating from the mean value is much higher than that in a normal distribution.

The dominate mode frequency is further analysed from another perspective by separating the inter-area oscillations from different years and performing statistical analysis on the dominant mode frequency for each year. Fig. 9 compares the dominant mode frequency distribution of inter-area oscillations in different years. From Fig. 9, it can be seen that dominant mode frequency around 0.2 Hz attains the highest occurrence among all modes in each year. This is consistent with the results from Fig. 8. To further explore the dominant mode frequencies' centres, a simple *k*-means clustering algorithm was employed and the centroid mode frequency of each year is summarised in Table 2. From Table 2, it can be observed that two centres are located at 0.2 and 0.4 Hz, which indicate most of the inter-area oscillations have the oscillation modes 0.2 and 0.4 Hz within the EI system.

Similar to the hourly analysis on dominant mode frequency distribution in the previous section, damping ratios of each detected inter-area oscillation in EI are grouped into 24 h and the hourly distribution of damping ratio is shown in Figs. 10 and 11. In each hour, median damping ratio is calculated and presented in Fig. 10.

From Fig. 10*a*, it can be seen that the majority of damping ratios is below 30% over 6 years. The median damping ratios in different years have few variations, except the year 2013 when a relatively higher median damping ratio is observed. The area of damping ratio which is close to 10% may follow a normal distribution, whereas other regions of damping ratio show significant deviations from the normal distribution.

Fig. 11 presents the centre of the damping ratios in the EI system. The centres of the damping ratio can be calculated by either statistical histogram or previously mentioned *k*-means clustering algorithm. As can be seen from Fig. 11, most of the oscillations in EI have a damping ratio larger than 10%, which indicate this system has a good capability to suppress inter-area oscillations.

5 Inter-area oscillation excitation types

Inter-area oscillations can be excited by power system disturbances such as generation trip. By comparing the system frequency before and after the disturbance, the excitations of oscillations captured by FNET/GridEye can be simply classified into several categories including generation trip, load shedding, line trip, and non-obvious reasons. Oscillations caused by the first three types of excitations, i.e. generation trip, load shedding, and line trip, are relatively easy to be identified since these oscillations have distinct features in terms of frequency and phase angle [35]. Therefore, this

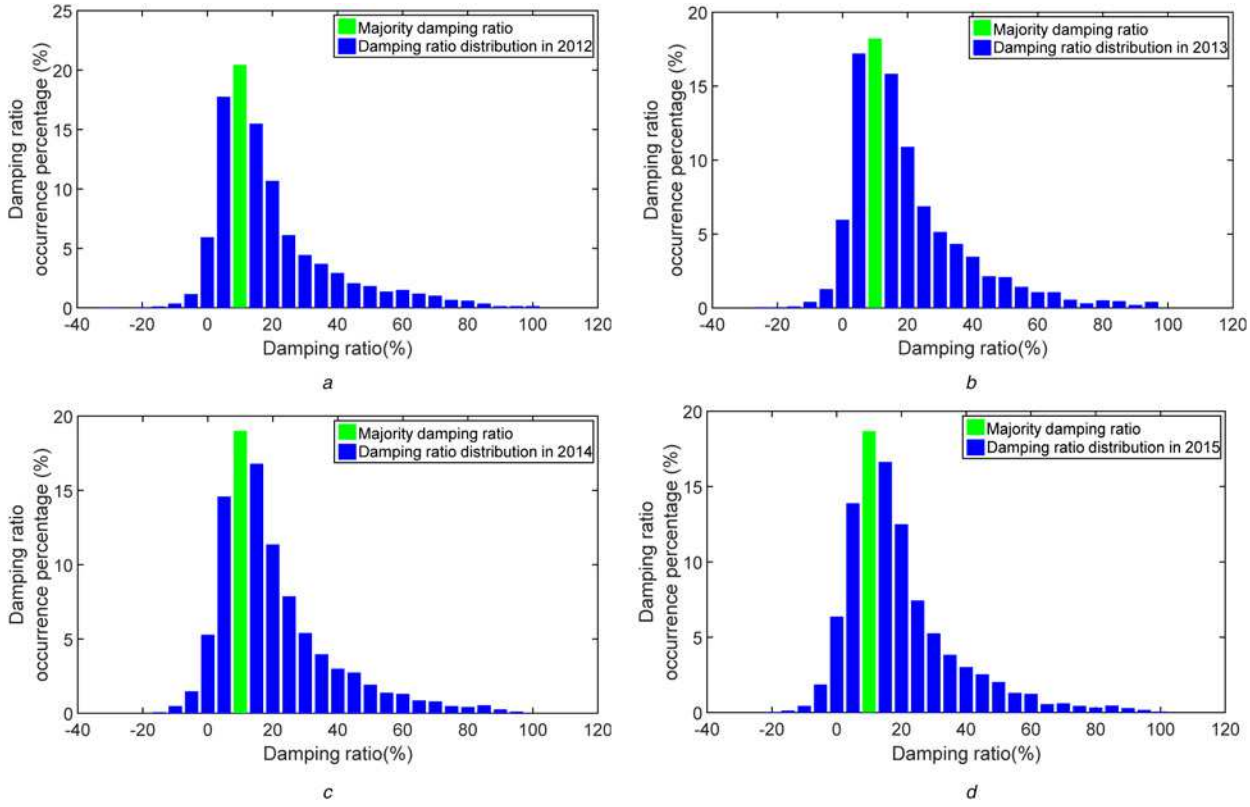

Fig. 11 *Damping ratio distribution of annual inter-area oscillations in EI*
a Damping ratio distribution of EI in 2012
b Damping ratio distribution of EI in 2013
c Damping ratio distribution of EI in 2014
d Damping ratio distribution of EI in 2015

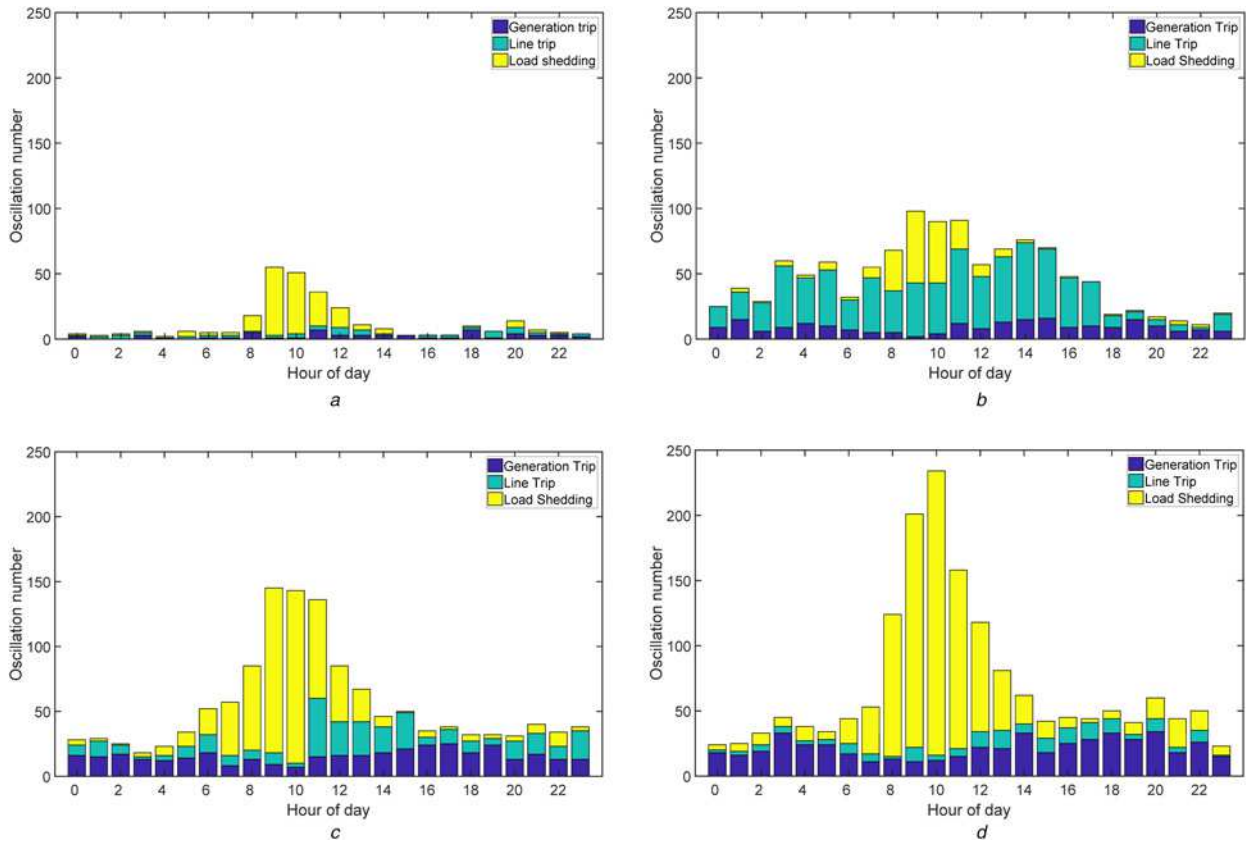

Fig. 12 *Occurrence of EI oscillations caused by different types of events*
a Oscillation events type of EI in 2012
b Oscillation events type of EI in 2013
c Oscillation events type of EI in 2014
d Oscillation events type of EI in 2015

section focuses on the statistical analysis on these three oscillation excitation types.

Fig. 12 shows the amount of oscillations excited by different types of disturbances (grouped into 24 h) from 2012 to 2015. From Fig. 12, it can be seen that the oscillation occurrence excited by different types of disturbance has similar distributions. Most of the oscillations are resulted from load reduction, except the year 2013. In 2013, during low load hours (from 8 am to 11 am UTC time), more inter-area oscillations are caused by line trip disturbance while for other hours, majority oscillations are caused by generation trip disturbance. Since some of the oscillation excitations are not obvious, further studies are required to investigate the causes of the oscillations that are currently hard to be recognised.

6 Conclusion

This paper conducted a preliminary statistical investigation on the inter-area oscillations that occurred in the EI system from 2010 and 2015. It focused on the inter-area oscillations with high magnitudes that can be easily observed using PUs. It discovered a strong association between system oscillations and load profiles. During a day, the system operating in low inertia hours is more vulnerable to inter-area oscillations than in heavy inertia hours. Similarly, during summer peak and winter peak, the system seems to be under lower risk of inter-area oscillations than shoulder seasons. Two centroids of dominate mode frequency are found to be 0.2 and 0.4 Hz in EI. In recent years, load reduction takes the majority proportion of confirmed oscillation excitations. Future work would focus on analysing more historical oscillations data and the excitations of non-obvious oscillations.

7 Acknowledgments

This work was supported primarily by the Engineering Research Centre Program of the National Science Foundation and the Department of Energy under NSF award number EEC-1041877 and the CURENT Industry Partnership Program.

8 References

[1] Liu Y., Yao W., Zhou D., *ET AL.*: 'Recent developments of FNET/GridEye – a situational awareness tool for smart grid', *CSEE J. Power Energy Syst.*, 2016, **2**, (3), pp. 19–27
[2] Sun K., Zhou Q., Liu Y.: 'A phase locked loop-based approach to real-time modal analysis on synchrophasor measurements', *IEEE Trans. Smart Grid*, 2014, **5**, (1), pp. 260–269
[3] Kamwa I., Grondin R., Hebert Y.: 'Wide-area measurement based stabilizing control of large power systems – a decentralized/hierarchical approach', *IEEE Trans. Power Syst.*, 2001, **16**, (1), pp. 136–153
[4] Majumder R., Pal B.C., Dufour C., *ET AL.*: 'Design and real-time implementation of robust FACTS controller for damping inter-area oscillation', *IEEE Trans. Power Syst.*, 2006, **21**, (2), pp. 809–816
[5] Zhang Y., Markham P., Xia T., *ET AL.*: 'Wide-area frequency monitoring network (FNET) architecture and applications', *IEEE Trans. Smart Grid*, 2010, **1**, (2), pp. 159–167
[6] Shiri F., Mohammadi-ivatloo B.: 'Identification of inter-area oscillations using wavelet transform and phasor measurement unit data', *Int. Trans. Electr. Energy*, 2015, **25**, (11), pp. 2831–2846
[7] Lauria D., Pisani C.: 'On Hilbert transform methods for low frequency oscillations detection', *IET Gener. Transm. Distrib.*, 2014, **8**, (6), pp. 1061–1074
[8] Liu Z., Zhang Q.: 'An approach to recognize the transient disturbances with spectral kurtosis', *IEEE Trans. Instrum. Meas.*, 2014, **63**, (1), pp. 46–55

[9] Peng J.C., Nair N.C.: 'Enhancing Kalman filter for tracking ring-down electromechanical oscillations', *IEEE Trans. Power Syst.*, 2012, **27**, (2), pp. 1042–1050
[10] Moravej Z., Pazoki M., Niasati M., *ET AL.*: 'A hybrid intelligence approach for power quality disturbances detection and classification', *Int. Trans. Electr. Energy*, 2013, **23**, (7), pp. 914–929
[11] Liu Y., Zhan L.W., Zhang Y., *ET AL.*: 'Wide-area-measurement system development at the distribution level: an FNET/GridEye example', *IEEE Trans. Power Deliv.*, 2016, **31**, (2), pp. 721–731
[12] Yang D., Rehtanz C., Li Y., *ET AL.*: 'A hybrid method and its applications to analyse the low frequency oscillations in the interconnected power system', *IET Gener. Transm. Distrib.*, 2013, **7**, (8), pp. 874–884
[13] Jiang T., Bai L., Li F., *ET AL.*: 'Synchrophasor measurement-based correlation approach for dominant mode identification in bulk power systems', *IET Gener. Transm. Distrib.*, 2016, **10**, (11), pp. 2710–2719
[14] Bai F., Zhu L., Liu Y., *ET AL.*: 'Design and implementation of a measurement-based adaptive wide-area damping controller considering time delays', *Electr. Power Syst. Res.*, 2016, **130**, pp. 1–9
[15] Hauer J.F., Demeure C., Scharf L.: 'Initial results in Prony analysis of power system response signals', *IEEE Trans. Power Syst.*, 1990, **5**, (1), pp. 80–90
[16] Xia T., Zhang Y., Chen L., *ET AL.*: 'Phase angle-based power system inter-area oscillation detection and modal analysis', *Eur. Trans. Electr. Power*, 2011, **21**, (4), pp. 1629–1639
[17] You S., Guo J., Kou G., *ET AL.*: 'Oscillation mode identification based on wide-area ambient measurements using multivariate empirical mode decomposition', *Electr. Power Syst. Res.*, 2016, **134**, pp. 158–166
[18] Wies R.W., Pierre J.W., Trudnowski D.J.: 'Use of ARMA block processing for estimating stationary low-frequency electromechanical modes of power systems', *IEEE Trans. Power Syst.*, 2003, **18**, (1), pp. 167–173
[19] De Moor B., Van Overschee P.: 'Numerical algorithms for subspace state space system identification (N4SID)'. Proc. ASME Design Engineering Technical Conf., Sacramento, CA, 1997, pp. 1–9
[20] Kamwa I., Gerin-Lajoie L.: 'State-space system identification – toward MIMO models for modal analysis and optimization of bulk power systems', *IEEE Trans. Power Syst.*, 2000, **15**, (1), pp. 326–335
[21] Fernandes L., da Costa E.: 'Estimation of dominant mode parameters in power systems using correlation analysis', *Electr. Power Syst. Res.*, 2017, **148**, pp. 295–302
[22] Fan L.: 'Data fusion-based distributed Prony analysis', *Electr. Power Syst. Res.*, 2017, **143**, pp. 634–642
[23] Wadduwage D., Annakkage U., Narendra K.: 'Identification of dominant low-frequency modes in ring-down oscillations using multiple Prony models', *IET Gener. Transm. Distrib.*, 2015, **9**, (15), pp. 2206–2214
[24] Zhou N., Pierre J., Trudnowski D.: 'A stepwise regression method for estimating dominant electromechanical modes', *IEEE Trans. Power Syst.*, 2012, **27**, (2), pp. 1051–1059
[25] Hwang J., Liu Y.: 'Identification of interarea modes from ring-down data by curve-fitting in the frequency domain', *IEEE Trans. Power Syst.*, 2017, **32**, (2), pp. 842–851
[26] Seppanen J., Au S., Turunen J., *ET AL.*: 'Bayesian approach in the modal analysis of electromechanical oscillations', *IEEE Trans. Power Syst.*, 2017, **32**, (1), pp. 316–325
[27] Yang D., Wang B., Cai G., *ET AL.*: 'Oscillation mode analysis for power grids using adaptive local iterative filter decomposition', *Int. J. Electr. Power Energy Syst.*, 2017, **92**, pp. 25–33
[28] Serna J., Ramirez J., Mendez A., *ET AL.*: 'Identification of electromechanical modes based on the digital Taylor–Fourier transform', *IEEE Trans. Power Syst.*, 2016, **31**, (1), pp. 206–215
[29] Yazdanian M., Mehrizi-Sani A., Mojiri M.: 'Estimation of electromechanical oscillation parameters using an extended Kalman filter', *IEEE Trans. Power Syst.*, 2015, **30**, (6), pp. 2994–3002
[30] Sarmadi S., Venkatasubramanian V.: 'Electromechanical mode estimation using recursive adaptive stochastic subspace identification', *IEEE Trans. Power Syst.*, 2014, **29**, (1), pp. 349–358
[31] Bai F., Liu Y., Liu Y., *ET AL.*: 'Measurement-based correlation approach for power system dynamic response estimation', *IET Gener. Transm. Distrib.*, 2015, **9**, (12), pp. 1474–1484
[32] Lee J., Kim H.: 'Selecting sampling interval of transient response for the improved Prony method', *IEEE Trans. Antennas Propag.*, 2003, **51**, (1), pp. 74–77
[33] 'U.S. electric system is made up of interconnections and balancing authorities'. Available at http://www.eia.gov/todayinenergy/detail.php?id=27152, accessed 1 December 2016
[34] Yu Y., Grijalva S., Thomas J.J., *ET AL.*: 'Oscillation energy analysis of inter-area low-frequency oscillations in power systems', *IEEE Trans. Power Syst.*, 2016, **31**, (2), pp. 1195–1203
[35] Zhang K., Ye Y., Chen L., *ET AL.*: 'FNET observations of low frequency oscillations in the eastern interconnection and their correlation with system events'. Proc. IEEE Power and Energy Society General Meeting (PESGM), Detroit, MI, USA, 2011, pp. 1–8